Ca²⁺-Facilitated Adhesion of Bacteria on the Na-Montmorillonite Surface

Yongshuai Sun* and Anping Lei

Read Online

ACCESS | Metrics & More | Article Recommendations
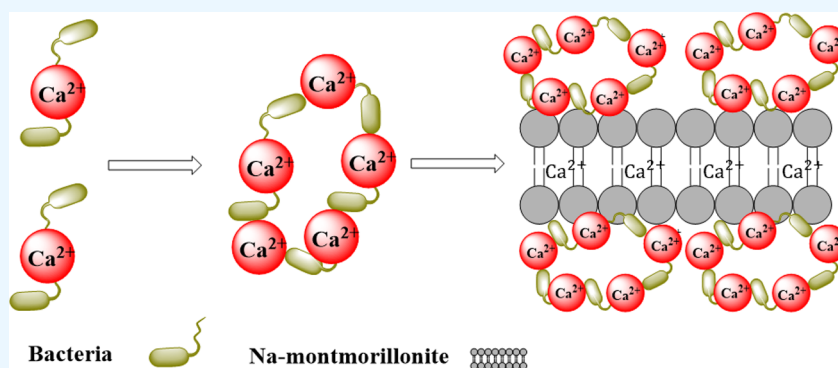
ABSTRACT: The adhesion of bacteria on clay surfaces strongly affected their migration and distribution in soil and water. Bacterial adhesion experiments on the Na-montmorillonite (Na-MMT) surface were conducted to determine the role of Na-MMT in the bacterial adhesion process and to prove the validity of the isotherm and kinetic theory for the bacterial surface adhesion in the presence of Ca²⁺ ions. Batch adhesion experiments with bacteria on the Na-MMT surface were carried out with varying time frames, temperatures, bacterial concentrations, and Ca²⁺ ion concentrations. The adhesion capacity of Na-MMT significantly correlated with the Ca²⁺ ion concentration, temperature, time frame, and bacterial concentration when Ca²⁺ ions were present. The adhesion morphology of the bacteria onto the Na-MMT surface, observed through the zeta-potential and atomic force microscopy (AFM), additionally demonstrated that the bacterial adhesion onto the Na-MMT surface was dominated by the nonelectrostatic force.

1. INTRODUCTION

The adhesion of bacteria onto clay surfaces is universal across water environments, soils, and sediments.[1] Meanwhile, microbial activity[2] and bacterial ecological distribution[3−5] can be significantly altered by this process. Biological colonies are formed when a certain number of bacteria cells adsorb on the clay surfaces,[6] and their establishment significantly affects soil's biological processes (aggregate formation, mineral weathering, and biodegradation of pollutants).[7] At the same time, the adhesion of bacteria on the clay surfaces also plays an important role in bacterial immobilization, affecting the migration of various pollutants[8−11] and the consolidation of sand through microbial-induced calcium carbonate precipitation (MICP).[12−15]

Studies of previous literature regarding the adhesion of bacteria onto mineral surfaces mainly focused on quartz, hematite, corundum, and so on.[16,17] The adhesion of bacteria onto the clay surfaces was affected by several steps, among which the initial adhesion was the critical one. Results showed that environmental factors (such as salt concentration, temperature, and pH) had a great influence on the initial adhesion.[18−20] For instance, the extent of the bacteria adhesion increased with the decreasing NaNO₃ concentration and pH. In the range of temperatures from 288 to 308 K,[21,22] the maximum adhesion extent of *Pseudomonas putida* onto the mineral surfaces was obtained. The adhesion extent of bacteria onto the similarly charged quartz increased with increasing salt concentrations.[23−25] However, the effect of ions on the adhesion mechanism of bacteria onto mineral surfaces has not been fundamentally approached or substantiated.

The adhesion and even distribution of bacteria are particularly important in sandy soil, which prevents the plugging of grouting points and ensures an even increase in soil strength due to the MICP process.[26−29] The process of bacterial immobilization was established in part by batch adhesion experiments using calcium ions and various materials

under a series of bio-geochemical reactions.[30−32] However, most previous studies revealed only the application effect of the MICP process, while neglecting the actual mechanism of adhesion. Because of this, more study is needed on the efficacy of economic and environmental-friendly adsorbents, as well as their respective adhesion mechanisms.

Calcium chloride as a calcium source was widely used[33−35] and played a tremendous role in the MICP process.[36−38] Meanwhile, the physical and chemical properties of clay minerals significantly affected Ca^{2+} ions.[39,40] For instance, the surface charge of clay minerals was changed by Ca^{2+} ions. In addition, the stoichiometric interaction between positively charged Ca^{2+} ions and the negatively charged bacterial wall was observed, which was beneficial to the adhesion of bacteria onto the surface of clay minerals and leads to an increase in the size of biomineral formed by MICP.[41] Earlier studies have shown that extracellular polymeric substances (EPS) secreted by bacteria could entrap Ca^{2+} ions.[42−45] The Ca^{2+} ions were adsorbed by EPS so that bacteria tend to be adsorbed onto clay surfaces containing Ca^{2+} ions.

Na-montmorillonite (Na-MMT) was a well-known double-layered clay mineral. It has many excellent material properties, such as a high specific surface, high cation exchange capacity, and low cost; because of this, it was widely used in many aspects of daily life.[46−49] Each crystal sheet of the Na-MMT consists of a central octahedral alumina sheet between two tetrahedral silicon sheets. Due to the substitution of Al^{3+} for Si^{4+} in the tetrahedral sheet and Mg^{2+} for Al^{3+} in the octahedral sheet, these crystal sheets retain a negative charge, which is counteracted through the adhesion of cations such as Na^+ and Ca^{2+}.[50,51] Na-MMT, as the main component of natural bentonite, was widely studied for use as a sorbent to ensure the immobilization of ionic liquids between clay layers.[48] Na-MMT could also immobilize uranyl peroxide nanoclusters onto the clay surface due to their favorable sorption and Na-MMT's high-specificity surface.[52] However, the adhesion mechanism of bacteria onto the Na-MMT surface was rarely researched, which played an important role in the MICP process and determined the application effect of MICP.

Therefore, this paper researched the adhesion mechanism of bacteria onto the Na-MMT surface to promote the development of MICP technology. This study examined the adhesion of bacteria onto the Na-MMT surface, and the influences that Ca^{2+} ion concentrations (2.7−13.5 mmol/L), temperatures (293−333 K), time frames (5−110 min), and bacterial concentrations (OD_{600} = 0.5−2.0) have on this process in both the presence and absence of Ca^{2+} ions. The adhesion capacity of bacteria onto the Na-MMT surface was examined using batch adhesion experiments. It was hypothesized that direct adhesion between Na-MMT and the bacteria would be impossible due to electrostatic repulsion between the negatively charged Na-MMT and bacterial surfaces.[53,54] However, the intercalation of cations on Na-MMT changes the surface charge of the material to make it possible for the negatively charged bacteria to interact with its surface. Further experiments were performed to determine if Ca^{2+} ions were able to promote the adhesion of the bacteria onto the Na-MMT surface. The adhesion mechanism of the material was characterized by Fourier transform infrared spectroscopy (FTIR), scanning electron microscopy (SEM), ζ-potential, and atomic force microscopy (AFM). Following this, the adhesion mechanisms, isotherm, and kinetic theory of bacterial adhesion onto the Na-MMT surface were further elucidated.

2. MATERIALS AND METHODS

2.1. Microorganisms and Growth Conditions. All chemicals were commercially obtained from Sinopharm Chemical Reagent Co, Ltd. (Shanghai, China). All reagents in this study were analytical grade and used without further purification. *Sporosarcina pasteurii* (ATCC11859) was tested for adhesion onto Na-MMT. The bacteria were cultured in a medium consisting of NaCl (5 g/L), urea (20 g/L), casein peptone (15 g/L), and soybean peptone (5 g/L) in 1000 mL of deionized water. The pH of the medium was approximately 7.3. The culture medium was sterilized at 121 °C for 30 min before the bacteria was incubated aerobically at 30 °C at 120 rpm for 48 h. The grown culture was centrifuged at 5434 g at 4 °C for 8 min to pellet the bacteria. The bacteria were washed three times with deionized water and were then suspended in 2.7, 5.4, 8.1, 10.8, and 13.5 mmol/L Ca^{2+} solution for future use and diluted to an optical density (OD_{600}) of 0.5, 1.0, 1.5, and 2.0.

The number of bacteria was expressed by measuring the absorbance of bacterial solution (turbidimetric method). The principle is mainly based on the fact that the bacterial concentration is directly proportional to the turbidity of the bacterial solution. Therefore, it is also directly proportional to the absorbance. In this paper, the absorbance of an ultraviolet−visible spectrophotometer (model UV-1700, Shimadzu company, Japan) at the wavelength of 600 nm was used to determine bacterial concentration. The actual bacterial concentration was converted by eq 1.[55]

$$Y = 8.59 \times 107 \cdot Z^{1.3627} \tag{1}$$

where Z is the OD_{600} value and Y is the bacterial concentration (mL^{-1}). However, this formula is used for conversion only when OD_{600} is between 0.2 and 0.8. When OD600 exceeds this range, it needs to be diluted before conversion. In this study, the OD_{600} value is usually used to express the bacterial concentrations directly.

2.2. Materials. The sample Na-MMT was provided by Zhejiang Fenghong New Materials Co., Ltd. Grading size distribution curves of Na-MMT are shown in Figure 1. The FTIR data was collected with an infrared spectrometer (FTIR8400, SHIMADZU, Japan) with a wavenumber range
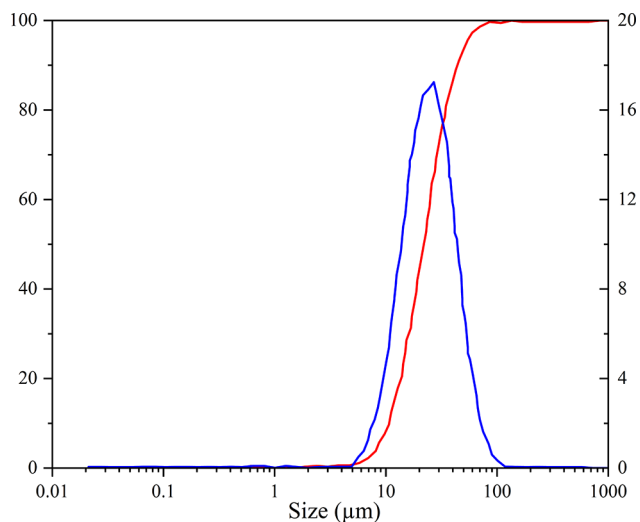
Figure 1. Grading size distribution curves of Na-MMT.

of 4000−400 cm^{-1}, scanning times of 32, and a resolution of 4 cm^{-1}. FTIR analysis data of Na-MMT is revealed in Figure 2.
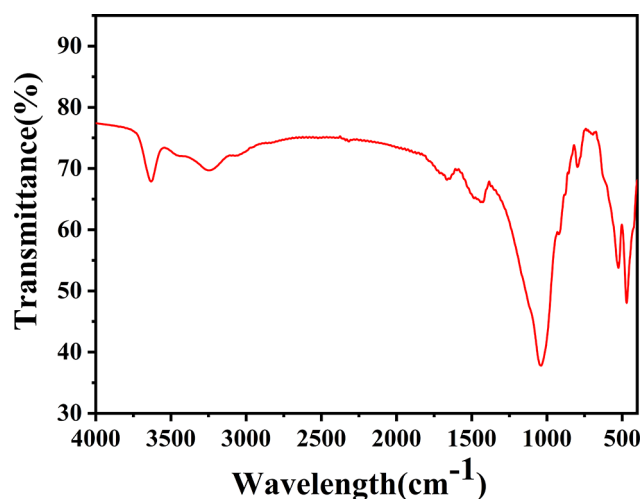
Figure 2. Characterization of Na-MMT investigated using FTIR.

The identification of Na-MMT was made by comparing the spectrum with the IR pattern catalogs (bands used in Table 1). Before the adsorption measurements, the sample was degassed at 120 °C for 8 h. The specific surface area of Na-MMT was 19.6012 m^2/g obtained by N$_2$ adsorption (Mike 2020).

Table 1. IR Bands for Na-MMT Used in FTIR

band (cm^{-1})	transmittance (%)	assignments
3636	65.9	Al−O−H
3468	70.8	H−O−H stretch
1640	74.1	H−O−H str.
1040	34.7	Si−O
916	64.7	Al−O−H str
796	76.8	Si−O str., Si−O−Al
524	48.5	Si−O str., Si−O−Al
468	41.2	Si−O, Si−O−Al

2.3. FTIR Spectroscopy. To determine whether the bacterial cells were adsorbed onto the Na-MMT surface, a sample was taken from the bacterial solution, Na-MMT, Na-MMT after incubation with Ca^{2+} ions, and Na-MMT adsorbed with bacteria in the presence of Ca^{2+} ions; all samples were separately placed in a mortar. Potassium bromide powder was added to the samples, and these substances were ground together. The ground sample was made into glass pieces using a tablet press; when the pressure was 10 Tcm^{-2}, the glass sample was taken off and then tested with FTIR (ftir8400, Shimadzu, Japan). Data was collected in the wavenumber range of 400−4000 cm^{-1}.

2.4. SEM and AFM. The collected samples of Na-MMT adsorbed with bacteria and without CaCl$_2$ were dried at 50 °C, and the morphology and microstructures were observed using SEM (Quanta-250, Germany). Before AFM analysis, the sample was dropped into the ethanol solution, and the dispersive solution was dropped onto the conductive ITO substrate after 10 min ultrasonic treatment. After drying, the nonelectrostatic forces of the Na-MMT surface with different concentrations of Ca^{2+} ions were tested through AFM. The force curve was obtained as follows: the tip was fixed at the free

end of the microcantilever. The sample was placed above the scanner, and then the piezoelectric ceramic tube of the scanner was moved by the driving voltage (V_p) in the direction perpendicular to the cantilever beam. The laser was emitted through the laser in the SPM probe, which shined on the back of the tip of the probe, and reflected the spot position detector. The voltage difference (V) was generated through the difference in light intensity between the upper and lower parts of the light spot position detector. The change amount of the spot position was obtained by measuring the voltage difference, as shown in Figure 3. When Na-MMT was vertically
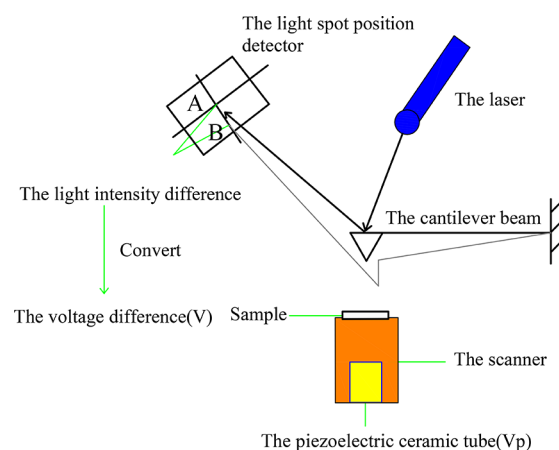
Figure 3. Schematic diagram of force curve measurement.

close to or far from the free end of the cantilever beam, a relative displacement occurred between the microcantilever and Na-MMT. In this process, the probe at the free end of the microcantilever was also approaching, or even pressing into the Na-MMT surface, and then detaching. Meanwhile, the force on the tip was measured and recorded by AFM to obtain the force curve.

The electrostatic force of the sample was tested in the EFM mode of AFM (EFM, Bruker Dimension Edge). This method mainly detected the charge distribution on the Na-MMT surface by the electrostatic interaction between the conductive probe and Na-MMT. During the test, the probe scans twice in the same line. The purpose of the first time was to observe the micromorphology of the Na-MMT surface by tapping mode. For the second time, according to the undulating track, the probe was lifted 100−200 nm and separated from Na-MMT, which ensured that the probe and Na-MMT were not affected by the short-range repulsive force and the roughness of the Na-MMT surface. Meanwhile, the probe and Na-MMT were mainly affected by the electrostatic force, which lead to changes in phase and amplitude. Therefore, the relative strength of the electrostatic force on the Na-MMT surface was obtained by phase. According to the experimental principle, the greater phase value meant a larger electrostatic force.

2.5. ζ-Potential. The ζ-potential values of Na-MMT and Na-MMT-CaCl$_2$ were measured by the ζ-potential analyzer (Malvern Zetasizer Nano ZS90). The Na-MMT and Na-MMT-CaCl$_2$ samples were dispersed in anhydrous ethanol with a concentration of 5−10 mg mL^{-1}. All experiments were repeated three times. The specific surface area of the minerals was obtained by N$_2$ adsorption (Mike 2020).

2.6. Batch Adhesion Experiments. Batch adhesion experiments were performed in triplicate by spiking 0.4 g of Na-MMT into a 100 mL solution containing 2.7, 5.4, 8.1, 10.8, and 13.5 mmol/L Ca^{2+} ions and bacteria. The experimental device diagram of the adhesion of bacteria onto the Na-MMT surface is shown in Figure 4. The reaction solution was stirred
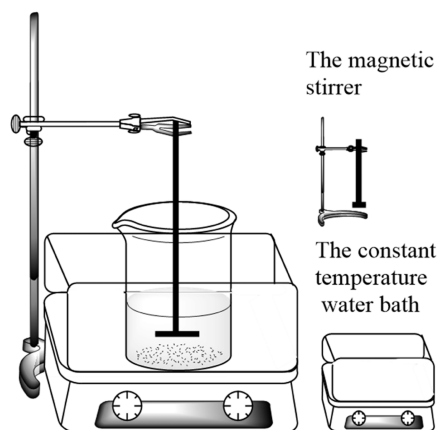
Figure 4. Experimental device diagram of the adhesion of bacteria onto the Na-MMT surface.

with a magnetic stirrer for 30 min at 240 r/min before reactors were sampled at various time frames and temperature points within (5−110 min; 293−333 K). More specifically, the adhesion of the bacteria ($OD_{600} = 1.0$) onto the Na-MMT surface at different concentrations of Ca^{2+} ions (2.7−13.5

mmol/L) was tested at 30 min, the adhesion of different bacterial concentrations (OD_{600} = 0.5, 1.0, 1.5, and 2.0) in the presence of 2.7 mmol/L Ca^{2+} ions was tested at 30 min, and the adhesion capacity of Na-MMT over various time points was monitored at different bacterial concentrations (OD_{600} = 0.5−2.0). The amount of bacteria adsorbed was calculated as the M value that was removed, according to eq (2), as the number of bacteria would be reduced after adhesion (where C_0 is the initial bacterial concentration and C_f is the concentration of bacteria after adhesion).

$$M(OD_{600}) = C_o - C_f \tag{2}$$

3. RESULTS AND DISCUSSION

3.1. Adhesion of Bacteria onto the Na-MMT Surface.
3.1.1. Effect of Contact Time. The adhesion of bacteria onto the Na-MMT surface with varying Ca^{2+} ion concentrations (2.7, 5.4, 8.1, 10.8, and 13.5 mmol/L) was found to increase over time (Figure 5a). The bacteria were found to adsorb slower in systems containing 2.7 mmol/L Ca^{2+} ions as compared to other concentrations, confirming that Ca^{2+} ions increase the bacterial adhesion rate onto Na-MMT. When Ca^{2+} ions were higher than 5.4 mmol/L, similar adhesion trends were observed, which may be because, at this point, most of the bacterial cells in the solution were already adsorbed.

3.1.2. Effect of Temperatures. When bacterial adhesion in the presence of Ca^{2+} (2.7, 5.4, 8.1, 10.8, and 13.5 mmol/L) was monitored, different temperatures adhesion on the Na-MMT surface increased as temperature increased at 2.7 mmol/L Ca^{2+} ions (Figure 5b), indicating that the adhesion rate was
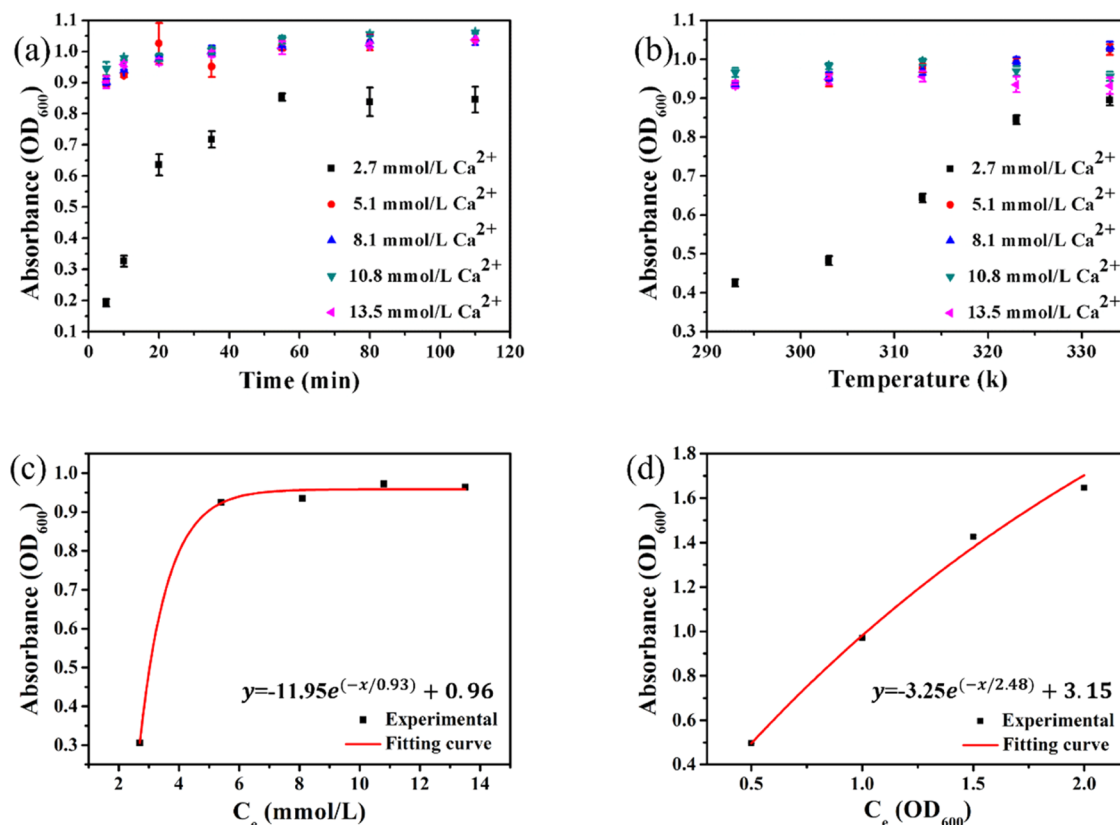
Figure 5. Effect of contact time (a), temperature (b), Ca^{2+} ion concentration (c), and bacterial concentration (d) on the adhesion of bacteria onto the Na-MMT surface.
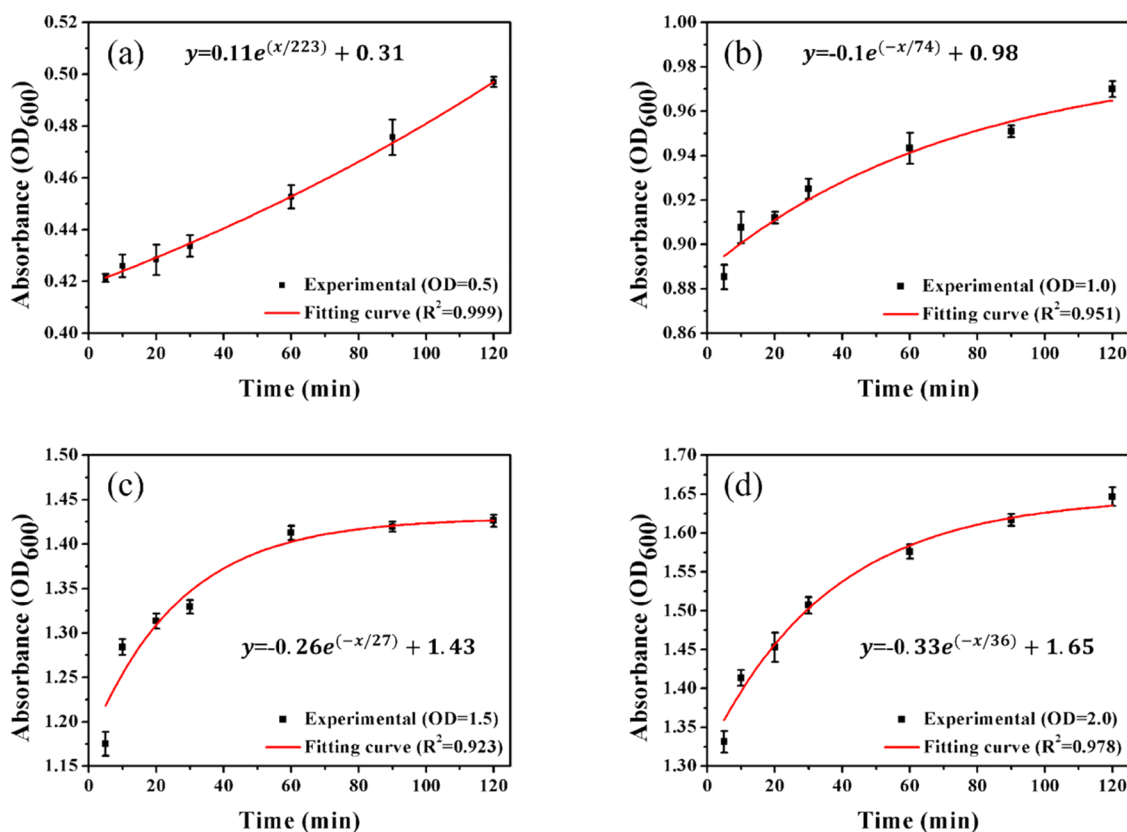
Figure 6. Effect of the initial bacterial concentration (OD = 0.5 (a), OD = 1.0 (b), OD = 1.5 (c), and OD = 2.0 (d)) on the adhesion of bacteria onto the Na-MMT surface over 110 min with 8.1 mmol/L Ca^{2+}.

improved by the temperature increase. However, in Ca^{2+} ion solutions, at 5.4, 8.1, 10.8, and 13.5 mmol/L, bacterial adhesion did not change significantly at different temperatures, this is likely because most of the bacteria in the solution were quickly adsorbed at higher concentrations of calcium; therefore, too few bacteria were left in solution, and the changing trend of bacterial adhesion extent was difficult to be observed with the increasing temperature.

3.1.3. Effect of Ca^{2+} Ion Concentrations. With the increasing Ca^{2+} ion concentrations, the adhesion capacity of the Na-MMT surface for the bacteria increased significantly (Figure 5c). At 5.4 mmol/L, the adhesion capacity reached the maximum value observed and did not increase with the further increase in Ca^{2+}, which was consistent with the results seen in previous tests (Figure 5a).

3.1.4. Effect of Bacterial Concentrations. According to the above experiment results, the adhesion of suspensions with different bacterial cell concentrations was monitored when the adhesion balance was reached (at 2 h). The effect of initial bacterial concentration on adhesion (between $OD_{600} = 0.5–2.0$) is shown in Figure 5d. The adhesion of the bacterial cells onto the Na-MMT surface increased almost linearly with the increase of bacterial concentration, demonstrating that Na-MMT has a strong adhesion extent for bacteria when Ca^{2+} ions were present, as saturation was not seen within the OD_{600} values tested.

3.1.5. Effect of Contact Time on Adhesion of Different Bacterial Concentrations. The effect of contact time over a range of 0–110 min on the adhesion of the bacteria was tested (Figure 6). The number of adsorbed bacteria onto the Na-MMT surface increased rapidly over time (0–110 min) in the

presence of 8.1 mmol/L Ca^{2+}. This rate was faster with increasing bacterial concentrations. The results demonstrated that a high initial concentration of bacteria can improve the adhesion rate of bacteria onto the Na-MMT surface.

3.2. Isotherm Studies and Kinetic Studies of Adhesion. *3.2.1. Isotherm Studies of Adhesion.* Two commonly used adhesion isotherm models were the Langmuir isotherm[56] and Freundlich isotherm. The equation of the Langmuir isotherm model is shown in eq (3), where q_e (OD_{600}) was the adhesion capacity at equilibrium, C_e (OD_{600}) was the equilibrium concentration of bacteria, q_{max} (OD_{600}) was the maximum adhesion capacity, and K_L was the effective dissociation constant.

$$\frac{C_e}{q_e} = \frac{1}{K_L q_{max}} + \frac{C_e}{q_{max}} \tag{3}$$

The Freundlich isotherm model was an empirical model used for heterogeneous adhesion,[57] the equation of which is shown in eq (4), where q_e (OD_{600}) was the adhesion capacity, C_e (OD_{600}) was the equilibrium concentration of bacteria, and $1/n$ and k_f were the indicators of adhesion intensity and adhesion capacity, respectively.

$$\ln q_e = \frac{1}{n} \ln C_e + \ln K_f \tag{4}$$

The experimental data fitted well to the Langmuir and Freundlich isotherm models. The fitted plot of C_e/q_e vs C_e is shown in Figure 7a, while the fitted plot of $\ln q_e$ vs $\ln C_e$ is shown in Figure 7b. The isotherm parameter data for the bacteria on the Na-MMT surface is listed in Table 2. The Langmuir and Freundlich models fitted the experimental data
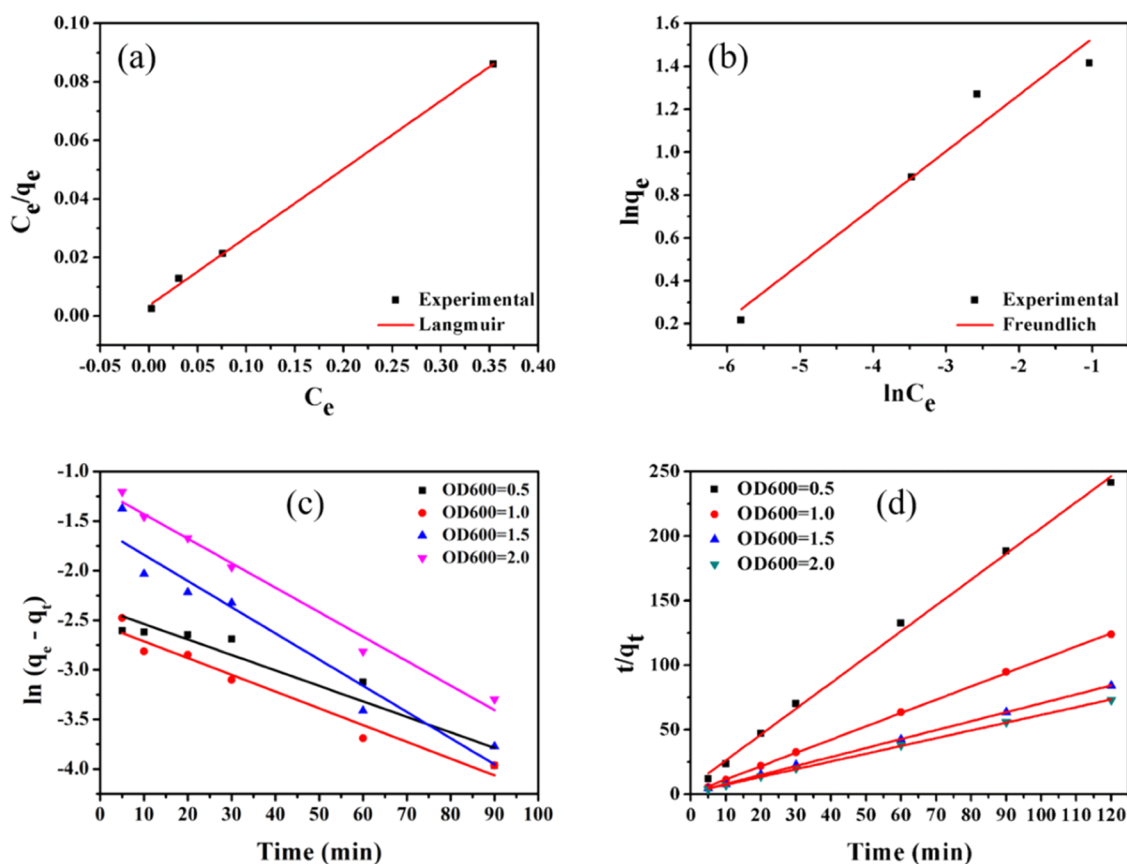
Figure 7. Langmuir (a) and Freundlich (b) isotherm models, and pseudo-first-order dynamics model (c) and pseudo-second-order dynamics model (d) for the adhesion of bacteria onto the Na-MMT surface in the presence of 8.1 mmol/L Ca^{2+}.

Table 2. Isotherm Parameter Values of Na-MMT

model	Langmuir			Freundlich		
parameter	q_{max}	K_L	R^2	n	k_f	R^2
	4.285	62.645	0.997	3.811	6.006	0.945

Table 3. Pseudo-First-Order Kinetic Models for the Adhesion of Bacteria onto the Na-MMT Surface

	pseudo-first-order	
bacteria	K_1	R_2
OD = 0.5	0.01563	0.89236
OD = 1.0	0.0169	0.9502
OD = 1.5	0.02642	0.92009
OD = 2.0	0.0247	0.98249

with correlation coefficients of $R^2 = 0.997$ and 0.945, respectively, indicating that the adhesion of the bacteria onto the Na-MMT surface followed these models. The results demonstrated that the bacteria was adsorbed to a high extent by Na-MMT in the presence of Ca^{2+}.

3.2.2. Kinetic Studies. The pseudo-first- and pseudo-second-order kinetic models of the bacterial adhesion were studied by examining the equilibrium adhesion capacity and the adhesion rate of the bacteria; these values were taken from when the concentration of bacteria was $OD_{600} = 0.5$, 1.0, 1.5, and 2.0. The rate equation of the pseudo-first-order kinetic model is shown in eq 5.

$$\ln(q_e - q_t) = \ln q_e - k_1 t \tag{5}$$

The values of q_e and K_1 can be calculated using the slope and intercept, respectively, and are listed in Table 3. Here, q_t was the number of bacteria adsorbed onto the Na-MMT surface at time t, q_e was the equilibrium adhesion capacity, and K_2 was the adhesion rate constant of the model. The fitted plot of $\ln(q_e - q_t)$ vs t is shown in Figure 7c.

The rate equation of the pseudo-second-order dynamics model is shown in eq 6.

$$\frac{t}{q_t} = \frac{1}{K_2 q_e^2} + \frac{t}{q_e} \tag{6}$$

The values of q_e and K_2 can be calculated using the slope and intercept, respectively, and are listed in Table 4. Here, q_t was the amount of the bacteria adsorbed onto the Na-MMT surface at time t, q_e was the equilibrium adhesion capacity, and K_2 was the adhesion rate constant of the model. The fitted plot of t/q_t vs t is shown in Figure 7(d).

Table 4. Pseudo-Second-Order Kinetic Models for the Adhesion of Bacteria onto the Na-MMT Surface

	pseudo-second-order			
bacteria	q_a	q_e	K_2	R^2
OD = 0.5	0.497 ± 0.008	0.500 ± 0.003	1.567	0.99724
OD = 1.0	0.969 ± 0.008	0.970 ± 0.006	0.943	0.99972
OD = 1.5	1.424 ± 0.016	1.449 ± 0.0015	0.427	0.99982
OD = 2.0	1.646 ± 0.034	1.667 ± 0.0023	0.261	0.99953
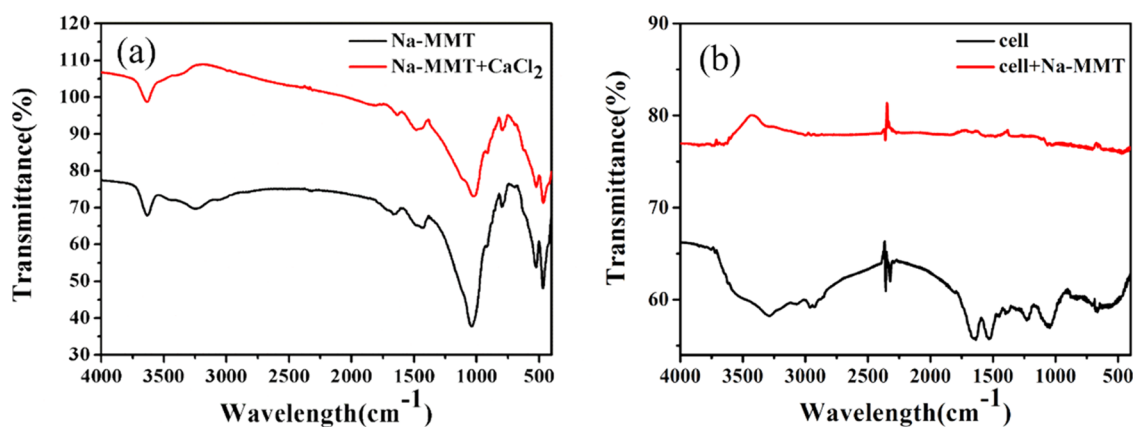
Figure 8. FTIR analysis of Na-MMT and Na-MMT after reaction with Ca^{2+} ions (a), bacteria, or Na-MMT adsorbed with bacteria in the presence of Ca^{2+} ions (b).
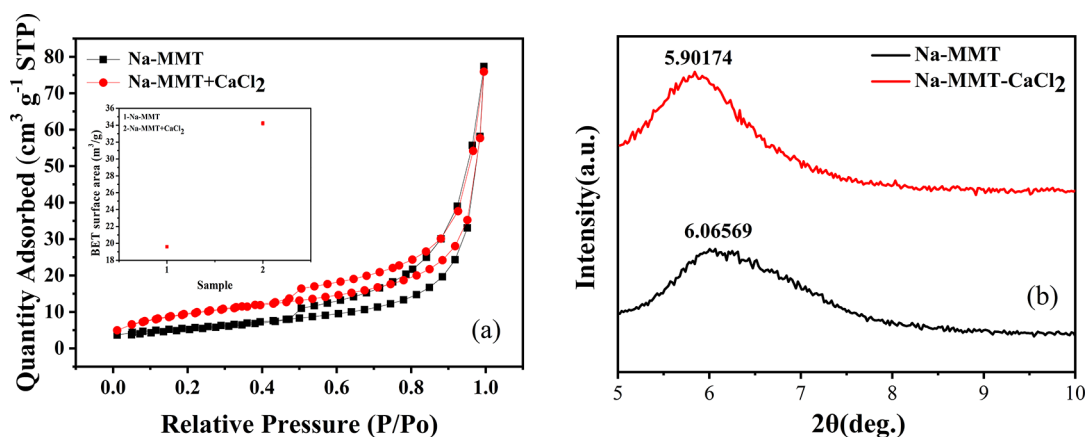
Figure 9. Specific surface area and cumulative volume of pores (a) and XRD data (b) of minerals (Na-MMT and Na-MMT-CaCl$_2$).

According to kinetic parameter values, the adhesion process of the bacteria onto the Na-MMT surface can be depicted by the pseudo-first-order kinetic and pseudo-second-order kinetic models. However, the correlation coefficient ($1 > R_2 > 0.99$) of the pseudo-second-order model (shown in Table 4) was higher than that ($0.98 > R_2 > 0.89$) of the pseudo-first-order model (shown in Table 3). Based on the values of the correlation coefficients R_2, it affirmed that the adhesion process of bacteria onto the Na-MMT surface could be better depicted by the pseudo-second-order kinetic model.

3.3. FTIR Analysis of the Bacteria on the Na-MMT Surface. The molecular groups of Na-MMT without Ca^{2+} ions, Na-MMT after reaction with Ca^{2+} ions, bacteria alone, and Na-MMT after bacteria adhesion in the presence of Ca^{2+} ions were all characterized using FTIR (Figure 8). The molecule groups of Na-MMT before and after the reaction with Ca^{2+} ions were found to be similar (Figure 8a), demonstrating that Ca^{2+} ions and the Na-MMT interactions were adsorptions of the cation with no additional chemical reactions. The adsorption bands of the bacteria were analyzed as follows: the peak at 1064 cm^{-1} in the curves can be assigned to the C−O bending from carboxylate ions (Zhan et al., 2014). The characteristic peak of 1534 cm^{-1} was attributed to the vibration of the amide II, N−H, or C−N from proteins. The peak at 1636 cm^{-1} confirmed the amide I (C=O) different conformation. The peaks at 2932 cm^{-1} were attributed to the CH$_2$ asymmetric stretching vibration from fatty acid. The symmetric stretching vibration ($\nu 1$ mode) of water molecules

was observed at 3362 cm^{-1}. For Na-MMT, the peaks at 470 and 524 cm^{-1} were assigned to the Si−O−Si bending vibration, and the strong peaks at 1040 cm^{-1} were attributed to the Si−O stretching vibrations. The peaks at 3632 and 1666 cm^{-1} were attributed to the symmetric stretching vibration ($\nu 1$ mode) and the bending vibrations ($\nu 2$ mode) of water molecules on the Na-MMT. No new peaks were obtained on the Na-MMT after bacteria adhesion in the presence of Ca^{2+} ions, compared with the peaks of Na-MMT, Na-MMT after reaction with Ca^{2+} ions, and bacteria. However, the vibrations of water molecules on Na-MMT shifted from 1666 to 1562 cm^{-1} and from 3632 to 3702 cm^{-1}, respectively, for $\nu 2$ and $\nu 1$ modes after the bacterial adhesion, which proved that the water molecules on Na-MMT are involved in bacterial adhesion. The frequency of the $\nu 1$ mode shifted to higher energies, while the $\nu 2$ mode shifted to lower energies, which were attributed to the formation of hydrogen bonding between the bacteria and Na-MMT.[58,59]

3.4. Specific Surface Area and ζ-Potential Values of Minerals. The specific surface area of Na-MMT increased in the presence of Ca^{2+} ions (Figure 9a). Meanwhile, the hysteresis loop of the isotherm adhesion line of Na-MMT followed an H3 type curve. The increase in the specific surface area was caused by Ca^{2+} ion intercalation. As shown in Figure 9b, the interlayer spacing of Na-MMT was increased significantly after the introduction of Ca^{2+} ions. The value of the specific surface area of Na-MMT-CaCl$_2$ was higher than
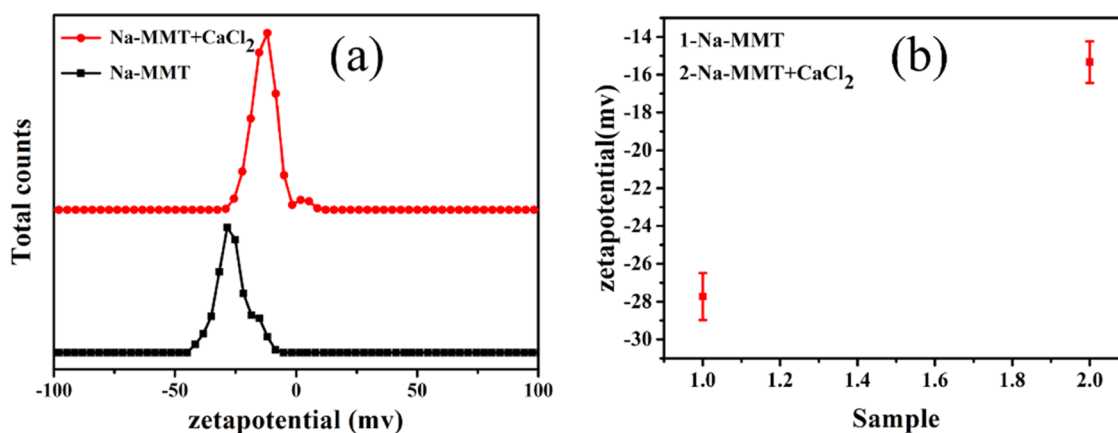
Figure 10. ζ-Potential value of Na-MMT in the absence and presence of Ca^{2+}.
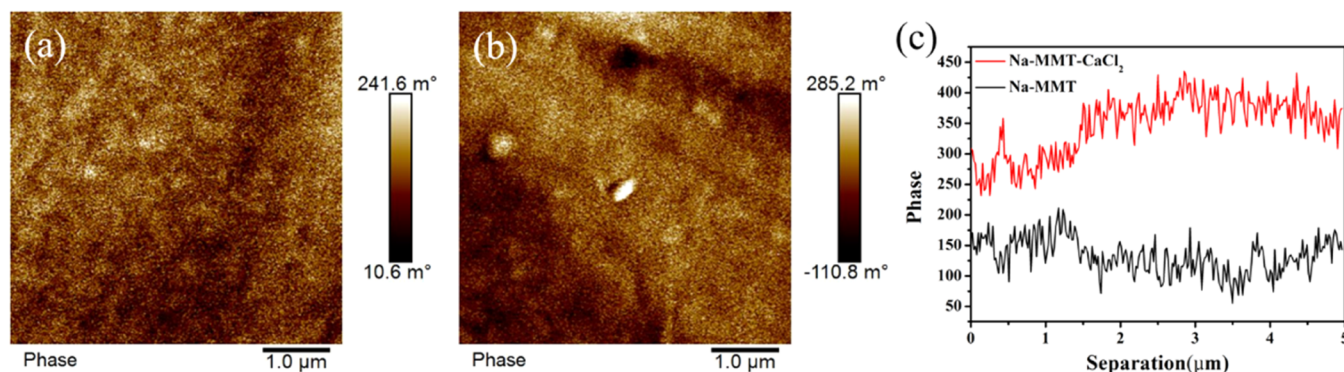
Figure 11. EFM image of Na-MMT (a) and Na-MMT-CaCl$_2$ (b) phases of the electrostatic force of Na-MMT and Na-MMT-CaCl$_2$ (c).
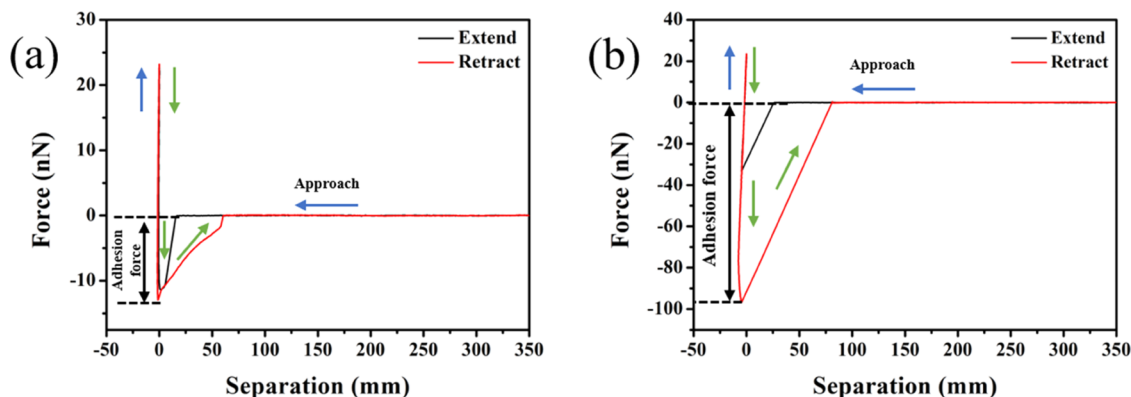
Figure 12. Force curve of Na-MMT (a) and Na-MMT-CaCl$_2$ (b).

that of Na-MMT, which could provide more accessible sites for bacterial adhesion on Na-MMT.

Figure 10 shows that the ζ-potential shifts from −26.3 to −14.2 mV in the presence of Ca^{2+} ions, accounting for the Na-MMT surface being negatively charged. Due to the negative charge of the Na-MMT surface and bacteria, we considered that electrostatic repulsion between the Na-MMT surface and bacteria was not conducive to bacterial adhesion onto the Na-MMT surface. The absolute value of the ζ-potential on Na-MMT in the presence of Ca^{2+} ions (14.2 mV) was smaller than that on Na-MMT (26.3 mV), explaining the adhesion force of the Na-MMT surface increases in the presence of Ca^{2+} ions compared with the absence of Ca^{2+} ions, which significantly

improved the adhesion extent of bacteria onto the Na-MMT surface.

3.5. EFM Analysis of Minerals. To evaluate the electrostatic force of pure Na-MMT and Na-MMT-CaCl$_2$, EFM was used at room temperature, as shown in Figure 11. The surface roughness of Na-MMT (R_a = 3.4) in Figure 11a was greater than that of Na-MMT-CaCl$_2$ (R_a = 2.8) in Figure 11b, indicating that Ca^{2+} ions changed the surface roughness on Na-MMT. Perera-Costa et al.[60] have reported that the increased surface roughness (1.86 < R_a < 7.89 μm) resulted in lower bacterial adhesion values. Therefore, the above result proved that Ca^{2+} ions promoted bacterial adhesion on the Na-MMT surface. Meanwhile, in Figure 11c, the phase value of Na-MMT-CaCl$_2$ and Na-MMT were positive, and the phase
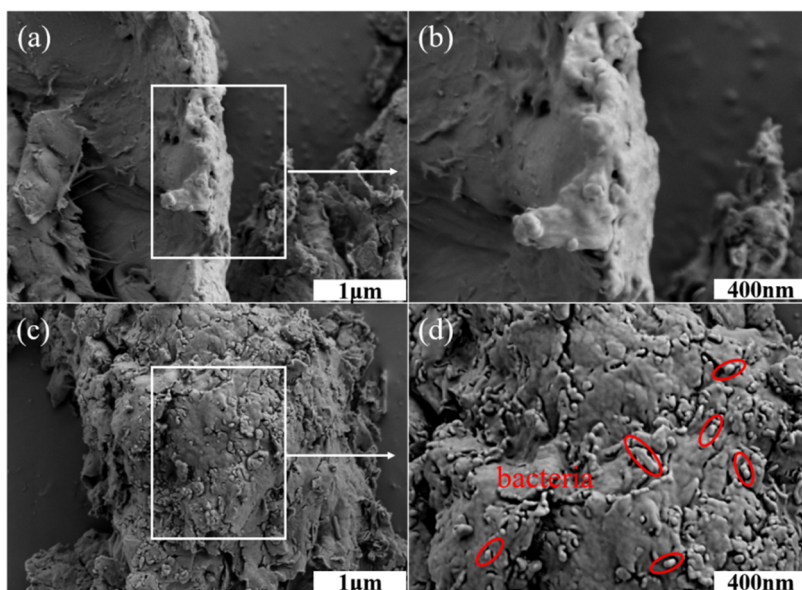
Figure 13. SEM analysis of the adhesion of bacteria onto the Na-MMT surface in the absence of Ca^{2+} ions (a, b) and in the presence of Ca^{2+} ions (c, d).

value of Na-MMT-CaCl$_2$ was greater than that of Na-MMT, indicating that the surface of Na-MMT presented greater electrostatic force in the presence of Ca^{2+} ions. Based on the ζ-potential results, the Na-MMT surface has more negative charges. However, the Na-MMT-CaCl$_2$ surface presented greater electrostatic force than Na-MMT. This was because the surface roughness of Na-MMT was greater than that of Na-MMT-CaCl$_2$, which caused the spacing between charges to increase. Therefore, a smaller electrostatic force was observed on the Na-MMT surface.

3.6. Force Curve Analysis of the Na-MMT Surface. To investigate the adhesion force of Na-MMT and Na-MMT-CaCl$_2$, the force curve experiment of Na-MMT and Na-MMT-CaCl$_2$ was conducted, as shown in Figure 12. The result indicated that the adhesion force of Na-MMT was 12.9 nN, whereas the adhesion force of Na-MMT-CaCl$_2$ was 96.72 nN, suggesting that the adhesion force of Na-MMT was enhanced by the introduction of Ca^{2+} ions. The above result was in agreement with the result of the ζ-potential. According to the result of EFM, Na-MMT had a smaller electrostatic force compared with that in the presence of Ca^{2+} ions. However, larger amounts of bacterial adhesion were observed on Na-MMT in the presence of Ca^{2+} ions, which implied that the nonelectrostatic forces might have played more important roles than the electrostatic force for bacterial adhesion on the Na-MMT surface. Zerda and Chattopadhyay[61,62] also found that virus adhesion onto silica and the adhesion of bacteriophages onto kaolinite were mainly governed by the nonelectrostatic forces.

3.7. SEM Analysis of the Adhesion of Bacteria on the Na-MMT Surface. To investigate the bacteria adhesion onto the Na-MMT surface, Na-MMT and bacteria in the absence of Ca^{2+} ions were visualized by SEM (Figure 13a,b), and Na-MMT and bacteria in the presence of Ca^{2+} ions were visualized by SEM (Figure 13c,d). Comparing the SEM graphs of the bacteria adhesion onto the Na-MMT surface with and without Ca^{2+} ions, almost no bacterial cells were found to be adsorbed onto the Na-MMT surface in the absence of Ca^{2+} ions (Figure 13b), while a large number of bacteria was adsorbed onto the

Na-MMT surface in the presence of Ca^{2+} ions (Figure 13d), which demonstrated that Ca^{2+} ions promoted the adhesion extent of bacteria onto the Na-MMT surface.

4. CONCLUSIONS

The adhesion of the bacteria to the Na-MMT surface was significantly affected by Ca^{2+} ions. The extent and rate of the bacterial adhesion onto Na-MMT surfaces can be improved by increasing the Ca^{2+} ion concentration, temperature, time frame, and initial bacterial concentration. The adhesion kinetics conformed to the pseudo-second-order kinetic model. The experimental values fitted the Langmuir and Freundlich isotherm models well. The result confirmed that the nonelectrostatic force and the electrostatic force of the Na-MMT surface were promoted by Ca^{2+} ions. Meanwhile, larger amounts of bacterial adhesion were observed on Na-MMT with Ca^{2+} ions, which proved the adhesion of bacteria onto the Na-MMT surface was dominated by the nonelectrostatic force. The morphology and microstructure of the bacteria on the Na-MMT surface also demonstrated that the adhesion extent of bacteria onto the Na-MMT surface was promoted by Ca^{2+} ions.

■ AUTHOR INFORMATION

Corresponding Author

Yongshuai Sun − *College of Water Resources & Civil Engineering, China Agricultural University, Beijing 100083, China;* ⊙ orcid.org/0000-0002-3641-9060; Email: causys666@163.com

Author

Anping Lei − *China Highway Engineering Consultants Corporation, Beijing 100089, China*

Complete contact information is available at:
https://pubs.acs.org/10.1021/acsomega.2c07260

Notes

The authors declare no competing financial interest.

The data that support the findings of this study are available from the corresponding author upon reasonable request.

■ REFERENCES

(1) Young, I. M.; Crawford, J. W. Interactions and self-organization in the soil-microbe complex. *Science* **2004**, *304*, 1634−1637.

(2) Schaeffer, A. J. Influence of interfaces on microbial activity. *Aktuelle Urol.* **1993**, *24*, 317−319.

(3) Reinert, L.; Batouche, K.; Leveque, J.-M.; Muller, F.; Beny, J.-M.; Kebabi, B.; Duclaux, L. Adsorption of imidazolium and pyridinium ionic liquids onto montmorillonite: Characterisation and thermodynamic calculations. *Chem. Eng. J.* **2012**, *209*, 13−19.

(4) Stotzky, G.; Rem, L. T. Influence of clay minerals on microorganisms. IV. Montmorillonite and kaolinites on fungi. *Can. J. Microbiol.* **1967**, *13*, 1535−1550.

(5) Marshall, K. C. *Interfaces in Microbial Ecology*; Harvard University Press, 2014; Vol. *123*, p 344.

(6) Nannipieri, P.; Ascher, J.; Ceccherini, M. T.; Landi, L.; Pietramellara, G.; Renella, G. Microbial diversity and soil functions. *Eur. J. Soil Sci.* **2017**, *68*, 12−26.

(7) Chenu, C.; G, S. *Interactions Between Microorganisms and Soil Particles*; John Wiley & Sons Ltd., 2002; pp 3−40.

(8) Yee, N.; Fein, J. B. Does metal adsorption onto bacterial surfaces inhibit or enhance aqueous metal transport? Column and batch reactor experiments on Cd-*Bacillus subtilis*-quartz systems. *Chem. Geol.* **2002**, *185*, 303−319.

(9) Mills, A. L.; Herman, J. S.; Hornberger, G. M.; Dejesus, T. H. Effect of solution ionic strength and iron coatings on mineral grains on the sorption of bacterial cells to quartz sand. *Appl. Environ. Microbiol.* **1994**, *60*, 3300−3306.

(10) Jacobs, A.; Lafolie, F.; Herry, J. M.; Debroux, M. Kinetic adhesion of bacterial cells to sand: Cell surface properties and adhesion rate. *Colloids Surf., B* **2007**, *59*, 35−45.

(11) Morrow, J. B.; Stratton, R.; Yang, H. H.; Smets, B. F.; Grasso, D. Macro- and manoscale observations of adhesive behavior for several *E. coli* strains (O157: H7 and environmental isolates) on mineral surfaces. *Environ. Sci. Technol.* **2005**, *39*, 6395−6404.

(12) Hao, Y. F.; Cheng, L.; Hao, H.; Shahin, M. A. Enhancing fiber/matrix bonding in polypropylene fiber reinforced cementitious composites by microbially induced calcite precipitation pre-treatment. *Cem. Concr. Compos.* **2018**, *88*, 1−7.

(13) Feng, K.; Montoya, B. M. Quantifying Level of Microbial-Induced Cementation for Cyclically Loaded Sand. *J. Geotech. Geoenviron. Eng.* **2017**, *143*, No. 06017005.

(14) Muhammad, N. Z.; Shafaghat, A.; Keyvanfar, A.; Majid, M. Z. A.; Ghoshal, S. K.; Yasouj, S. E. M.; Ganiyu, A. A.; Kouchaksaraei, M. S.; Kamyab, H.; Taheri, M. M.; Shirdar, M. R.; McCaffer, R. Tests and methods of evaluating the self-healing efficiency of concrete: A review. *Constr. Build. Mater.* **2016**, *112*, 1123−1132.

(15) Cheng, L.; Cord-Ruwisch, R. Upscaling Effects of Soil Improvement by Microbially Induced Calcite Precipitation by Surface Percolation. *Geomicrobiol. J.* **2014**, *31*, 396−406.

(16) Yee, N.; Fein, J. B.; Daughney, C. J. Experimental study of the pH, ionic strength, and reversibility behavior of bacteria-mineral adsorption. *Geochim. Cosmochim. Acta* **2000**, *64*, 609−617.

(17) Lin, F. Y.; Chen, C. S.; Chen, W. Y.; Yamamoto, S. Microcalorimetric studies of the interaction mechanisms between proteins and Q-Sepharose at pH near the isoelectric point (pI) - Effects of NaCl concentration, pH value, and temperature. *J. Chromatogr. A* **2001**, *912*, 281−289.

(18) Ruan, B.; Wu, P. X.; Liu, J.; Jiang, L.; Wang, H. M.; Qiao, J. L.; Zhu, N. W.; Dang, Z.; Luo, H. J.; Yi, X. Y. Adhesion of *Sphingomonas* sp. GY2B onto montmorillonite: A combination study by thermodynamics and the extended DLVO theory. *Colloids Surf., B* **2020**, *192*, No. 111085.

(19) Hong, Z.; Rong, X.; Cai, P.; Liang, W.; Huang, Q. Effects of Temperature, pH and Salt Concentrations on the Adsorption of *Bacillus subtilis* on Soil Clay Minerals Investigated by Microcalorimetry. *Geomicrobiol. J.* **2011**, *28*, 686−691.

(20) Hong, Z. N.; Jiang, J.; Li, J. Y.; Xu, R. K. Preferential adhesion of surface groups of *Bacillus subtilis* on gibbsite at different ionic strengths and pHs revealed by ATR-FTIR spectroscopy. *Colloids Surf., B* **2018**, *165*, 83−91.

(21) Jiang, D.; Huang, Q.; Cai, P.; Rong, X.; Chen, W. Adsorption of *Pseudomonas putida* on clay minerals and iron oxide. *Colloids Surf., B* **2007**, *54*, 217−221.

(22) Costa, R. C.; Souza, J. G. S.; Cordeiro, J. M.; Bertolini, M.; de Avila, E. D.; Landers, R.; Rangel, E. C.; Fortulan, C. A.; Retamal-Valdes, B.; da Cruz, N. C.; Feres, M.; Barao, V. A. R. Synthesis of bioactive glass-based coating by plasma electrolytic oxidation: Untangling a new deposition pathway toward titanium implant surfaces. *J. Colloid Interface Sci.* **2020**, *579*, 680−698.

(23) Wang, H. M.; Yang, Y. H.; Zhao, W. W.; Han, Y.; Luo, J.; Zhao, X.; Zhang, H. Y. Bioinspired Polymeric Coating with Self-Adhesion, Lubrication, and Drug Release for Synergistic Bacteriostatic and Bactericidal Performance. *Adv. Mater. Interfaces* **2022**, *9*, No. 2200561.

(24) Wu, D.; He, L.; Ge, Z.; Tong, M. P.; Kim, H. Different electrically charged proteins result in diverse bacterial transport behaviors in porous media. *Water Res.* **2018**, *143*, 425−435.

(25) Zuki, F. M.; Edyvean, R. G. J.; Ali, U. F. M.; Pourzolfaghar, H.; Gafri, H. F. S.; Bzour, M. I. The impact of ionic strength and pH on the interaction of *Pseudomonas putida* to minerals and electrical potential of surfaces. *Desalin. Water Treat.* **2022**, *249*, 191−203.

(26) Whiffin, V. S.; van Paassen, L. A.; Harkes, M. P. Microbial carbonate precipitation as a soil improvement technique. *Geomicrobiol. J.* **2007**, *24*, 417−423.

(27) Wang, Y. Z.; Soga, K.; Dejong, J. T.; Kabla, A. J. A microfluidic chip and its use in characterising the particle-scale behaviour of microbial-induced calcium carbonate precipitation (MICP). *Geotechnique* **2019**, *69*, 1086−1094.

(28) van Paassen, L. A.; Ghose, R.; van der Linden, T. J. M.; van der Star, W. R. L.; van Loosdrecht, M. C. M. Quantifying Biomediated Ground Improvement by Ureolysis: Large-Scale Biogrout Experiment. *J. Geotech. Geoenviron. Eng.* **2010**, *136*, 1721−1728.

(29) Torkzaban, S.; Tazehkand, S. S.; Walker, S. L.; Bradford, S. A. Transport and fate of bacteria in porous media: Coupled effects of chemical conditions and pore space geometry. *Water Resour. Res.* **2008**, *44*, No. W04403.

(30) Zhao, Y.; Fan, C. B.; Liu, P. H.; Fang, H. G.; Huang, Z. Q. Effect of activated carbon on microbial-induced calcium carbonate precipitation of sand. *Environ. Earth Sci.* **2018**, *77*, No. 615.

(31) Harkes, M. P.; van Paassen, L. A.; Booster, J. L.; Whiffin, V. S.; van Loosdrecht, M. C. M. Fixation and distribution of bacterial activity in sand to induce carbonate precipitation for ground reinforcement. *Ecol. Eng.* **2010**, *36*, 112−117.

(32) Cheng, L.; Cord-Ruwisch, R. In situ soil cementation with ureolytic bacteria by surface percolation. *Ecol. Eng.* **2012**, *42*, 64−72.

(33) De Muynck, W.; Cox, K.; De Belle, N.; Verstraete, W. Bacterial carbonate precipitation as an alternative surface treatment for concrete. *Constr. Build. Mater.* **2008**, *22*, 875−885.

(34) DeJong, J. T.; Mortensen, B. M.; Martinez, B. C.; Nelson, D. C. Bio-mediated soil improvement. *Ecol. Eng.* **2010**, *36*, 197−210.

(35) Pacheco-Torgal, F.; Labrincha, J. A. Biotech cementitious materials: Some aspects of an innovative approach for concrete with enhanced durability. *Constr. Build. Mater.* **2013**, *40*, 1136−1141.

(36) Liu, L.; Liu, H. L.; Xiao, Y.; Chu, J.; Xiao, P.; Wang, Y. Biocementation of calcareous sand using soluble calcium derived from calcareous sand. *Bull. Eng. Geol. Environ.* **2018**, *77*, 1781−1791.

(37) Chek, A.; Crowley, R.; Ellis, T. N.; Durnin, M.; Wingender, B. Evaluation of Factors Affecting Erodibility Improvement for MICP-Treated Beach Sand. *J. Geotech. Geoenviron. Eng.* **2021**, *147*, No. 04021001.

(38) Achal, V.; Pan, X. L. Influence of Calcium Sources on Microbially Induced Calcium Carbonate Precipitation by *Bacillus sp* CR2. *Appl. Biochem. Biotechnol.* **2014**, *173*, 307−317.

(39) Au, P. I.; Pillai, P.; Leong, Y. K. Ageing and collapse of Bentonite gels - Effects of Mg(II), Ca(II) and Ba(II) ions. *Appl. Clay Sci.* **2015**, *114*, 141−150.

(40) Tian, Z. F.; Tang, X. W.; Li, J.; Xiu, Z. L.; Xue, Z. J. Improving settlement and reinforcement uniformity of marine clay in electro-osmotic consolidation using microbially induced carbonate precipitation. *Bull. Eng. Geol. Environ.* **2021**, *80*, 6457−6471.

(41) Shirakawa, M. A.; Cincotto, M. A.; Atencio, D.; Gaylarde, C. C.; John, V. M. Effect of culture medium on biocalcification by *Pseudomonas Putida*, *Lysinibacillus Sphaericus* and *Bacillus Subtilis*. *Braz. J. Microbiol.* **2011**, *42*, 499−507.

(42) Ali, A.; Li, M.; Su, J. F.; Li, Y. F.; Wang, Z.; Bai, Y. H.; Ali, E. F.; Shaheen, S. M. *Brevundimonas diminuta* isolated from mines polluted soil immobilized cadmium (Cd2+) and zinc (Zn2+) through calcium carbonate precipitation: Microscopic and spectroscopic investigations. *Sci. Total Environ.* **2022**, *813*, No. 152668.

(43) Xiong, F. Z.; Wen, D. H.; Li, Q. L. Calcium-Mediated Regulation Promotes the Biofilm Formation of Two Novel Pyridine-Degrading Bacteria. *Front. Environ. Sci.* **2022**, *10*, No. 155.

(44) Wang, Z.; Su, J. F.; Ali, A.; Yang, W. S.; Zhang, R. J.; Li, Y. F.; Zhang, L. F.; Li, J. W. Chitosan and carboxymethyl chitosan mimic biomineralization and promote microbially induced calcium precipitation. *Carbohydr. Polym.* **2022**, *287*, No. 119335.

(45) Achal, V.; Mukherjee, A.; Basu, P. C.; Reddy, M. S. Strain improvement of *Sporosarcina pasteurii* for enhanced urease and calcite production. *J. Ind. Microbiol. Biotechnol.* **2009**, *36*, 981−988.

(46) Mehrabian, N.; Dariani, A. A. S. Anticorrosive performance of epoxy/modified clay nanocomposites. *Polym. Compos.* **2018**, *39*, E2134−E2142.

(47) Takahashi, C.; Shirai, T.; Fuji, M. Study on intercalation of ionic liquid into montmorillonite and its property evaluation. *Mater. Chem. Phys.* **2012**, *135*, 681−686.

(48) Pei, J. J.; Xing, X. S.; Xia, B. R.; Wang, Z. M.; Luo, Z. H. Study on the Adsorption Behavior between an Imidazolium Ionic Liquid and Na-Montmorillonite. *Molecules* **2019**, *24*, No. 1396.

(49) Narro-Céspedes, R. I.; Neira-Velazquez, M. G.; Mora-Cortes, L. F.; Hernandez-Hernandez, E.; Castaneda-Facio, A. O.; Ibarra-Alonso, M. C.; Reyes-Acosta, Y. K.; Soria-Arguello, G.; Borjas-Ramos, J. J. Surface Modification of Sodium Montmorillonite Nanoclay by Plasma Polymerization and Its Effect on the Properties of Polystyrene Nanocomposites. *J. Nanomater.* **2018**, *2018*, 1−13.

(50) Díaz, M.; Villa-García, M. A.; Duarte-Silva, R.; Rendueles, M. Preparation of organo-modified kaolinite sorbents: The effect of surface functionalization on protein adsorption performance. *Colloids Surf., A* **2017**, *530*, 181−190.

(51) Vinuth, M.; Naik, H. S. B.; Manjanna, J. Remediation of hexavalent chromium from aqueous solution using clay mineral Fe(II)-montmorillonite: Encompassing anion exclusion impact. *Appl. Surf. Sci.* **2015**, *357*, 1244−1250.

(52) Sadergaski, L. R.; Said, M.; Hixon, A. E. Calcium-Facilitated Aggregation and Precipitation of the Uranyl Peroxide Nanocluster U-60 in the Presence of Na-Montmorillonite. *Environ. Sci. Technol.* **2019**, *53*, 4922−4930.

(53) De Muynck, W.; De Belie, N.; Verstraete, W. Microbial carbonate precipitation in construction materials: A review. *Ecol. Eng.* **2010**, *36*, 118−136.

(54) Bundeleva, I. A.; Shirokova, L. S.; Benezeth, P.; Pokrovsky, O. S.; Kompantseva, E. I.; Balor, S. Zeta potential of anoxygenic phototrophic bacteria and Ca adsorption at the cell surface: Possible implications for cell protection from $CaCO_3$ precipitation in alkaline solutions. *J. Colloid Interface Sci.* **2011**, *360*, 100−109.

(55) Ramachandran, S. K.; Ramakrishnan, V.; Bang, S. S. Remediation of Concrete Using Microorganisms. *ACI Mater. J.* **2001**, *98*, 3−9.

(56) Langmuir, I. The constitution and fundamental properties of solids and liquids. Part II.-Liquids. *J. Franklin Inst.* **1917**, *184*, 721−730.

(57) Aşçı, Y.; Nurbas, M.; Açıkel, Y. S. A comparative study for the sorption of Cd(II) by soils with different clay contents and mineralogy and the recovery of Cd(II) using rhamnolipid biosurfactant. *J. Hazard. Mater.* **2008**, *154*, 663−673.

(58) Xue, W. H.; He, H. P.; Zhu, J. X.; Yuan, P. FTIR investigation of CTAB-Al-montmorillonite complexes. *Spectrochim. Acta, Part A* **2007**, *67*, 1030−1036.

(59) Xu, W. Z.; Johnston, C. T.; Parker, P.; Agnew, S. F. Infrared study of water sorption on Na-, Li-, Ca-, and Mg-exchanged (SWy-1 and SAz-1) montmorillonite. *Clays Clay Miner.* **2000**, *48*, 120−131.

(60) Perera-Costa, D.; Bruque, J. M.; Gonzalez-Martin, M. L.; Gomez-Garcia, A. C.; Vadillo-Rodriguez, V. Studying the Influence of Surface Topography on Bacterial Adhesion using Spatially Organized Microtopographic Surface Patterns. *Langmuir* **2014**, *30*, 4633−4641.

(61) Chattopadhyay, S.; Puls, R. W. Adsorption of bacteriophages on clay minerals. *Environ. Sci. Technol.* **1999**, *33*, 3609−3614.

(62) Zerda, K. S.; Gerba, C. P.; Hou, K. C.; Goyal, S. M. Adsorption of Viruses to Charge-modified silia. *Appl. Environ. Microbiol.* **1985**, *49*, 91−95.